

Interfacial stress engineering toward enhancement of ferroelectricity in Al doped HfO_2 thin films

S X Chen(陈思学), M M Chen(陈明明), Y Liu(刘圆), D W Cao(曹大威), and G J Chen(陈国杰)

Citation: Chin. Phys. B, 2024, 33 (**9**): 098701. DOI: 10.1088/1674-1056/ad4ff4
Journal homepage: http://cpb.iphy.ac.cn; http://iopscience.iop.org/cpb

What follows is a list of articles you may be interested in

Disorder-to-order transition induced by spontaneous cooling regulation in robotic active matter

Shuaixu Hou(侯帅旭), Gao Wang(王高), Xingyu Ma(马星宇), Chuyun Wang(汪楚云), Peng Wang(王鹏), Huaicheng Chen(陈怀城), Liyu Liu(刘雳宇), and Jing Wang(王璟)
Chin. Phys. B, 2024, 33 (**7**): 078701. DOI: 10.1088/1674-1056/ad4327

Orderly hysteresis in field-driven robot swarm active matter

Yanping Liu(刘艳萍), Gao Wang(王高), Peilong Wang(王培龙), Daming Yuan(袁大明), Shuaixu Hou(侯帅旭), Yangkai Jin(金阳凯), Jing Wang(王璟), and Liyu Liu(刘雳宇)
Chin. Phys. B, 2023, 32 (**6**): 068701. DOI: 10.1088/1674-1056/acc803

Any-polar resistive switching behavior in Ti-intercalated Pt/Ti/HfO_2/Ti/Pt device

Jin-Long Jiao(焦金龙), Qiu-Hong Gan(甘秋宏), Shi Cheng(程实), Ye Liao(廖晔), Shao-Ying Ke(柯少颖), Wei Huang(黄巍), Jian-Yuan Wang(汪建元), Cheng Li(李成), and Song-Yan Chen(陈松岩)
Chin. Phys. B, 2021, 30 (**11**): 118701. DOI: 10.1088/1674-1056/abf34e

Thermal properties of a two-dimensional intrinsically curved semiflexible biopolymer

Zicong Zhou(周子聪), Yanting Wang(王延颋)
Chin. Phys. B, 2017, 26 (**3**): 038701. DOI: 10.1088/1674-1056/26/3/038701

Plasticity-induced characteristic changes of pattern dynamics and the related phase transitions in small-world neuronal networks

Huang Xu-Hui (黄旭辉), Hu Gang (胡岗)
Chin. Phys. B, 2014, 23 (**10**): 108703. DOI: 10.1088/1674-1056/23/10/108703

Interfacial stress engineering toward enhancement of ferroelectricity in Al doped HfO_2 thin films

S X Chen(陈思学)[1], M M Chen(陈明明)[1,†], Y Liu(刘圆)[1], D W Cao(曹大威)[2], and G J Chen(陈国杰)[3]

[1] *Department of Microelectronics, Jiangsu University, Zhenjiang* 212013, *China*
[2] *Department of Physics, Jiangsu University, Zhenjiang* 212013, *China*
[3] *Guangdong–Hong Kong–Macao Joint Laboratory for Intelligent Micro-Nano Optoelectronic Technology, Foshan University, Foshan* 528225, *China*

(Received 28 January 2024; revised manuscript received 22 May 2024; accepted manuscript online 24 May 2024)

Ferroelectric HfO_2 has attracted much attention owing to its superior ferroelectricity at an ultra-thin thickness and good compatibility with Si-based complementary metal–oxide–semiconductor (CMOS) technology. However, the crystallization of polar orthorhombic phase (o-phase) HfO_2 is less competitive, which greatly limits the ferroelectricity of the as-obtained ferroelectric HfO_2 thin films. Fortunately, the crystallization of o-phase HfO_2 can be thermodynamically modulated via interfacial stress engineering. In this paper, the growth of improved ferroelectric Al doped HfO_2 (HfO_2:Al) thin films on (111)-oriented Si substrate has been reported. Structural analysis has suggested that nonpolar monoclinic HfO_2:Al grown on (111)-oriented Si substrate suffered from a strong compressive strain, which promoted the crystallization of (111)-oriented o-phase HfO_2 in the as-grown HfO_2:Al thin films. In addition, the in-plane lattice of (111)-oriented Si substrate matches well with that of (111)-oriented o-phase HfO_2, which further thermally stabilizes the o-phase HfO_2. Accordingly, an improved ferroelectricity with a remnant polarization ($2P_r$) of 26.7 μC/cm^2 has been obtained. The results shown in this work provide a simple way toward the preparation of improved ferroelectric HfO_2 thin films.

Keywords: improved ferroelectricity, interfacial stress engineering, compressive strain, HfO_2

PACS: 87.15.Zg, 64.60.Ej, 81.15.Gh, 61.05.cp **DOI:** 10.1088/1674-1056/ad4ff4

1. Introduction

Recently, ferroelectric hafnia (HfO_2) has been an important research subject due to its competitive advantages in ferroelectricity, such as superior ferroelectric properties at an ultra-thin thickness and large conceive electric field.[1] Meanwhile, the fabrication of ferroelectric HfO_2 thin films is well compatible with Si-based complementary metal–oxide–semiconductor (CMOS) technology, which makes them promising candidates for nonvolatile ferroelectric random-access memory and Moore-beyond ferroelectric field effect transistor devices.[2–4] It has been widely shown that the ferroelectricity in HfO_2 thin films is closely associated with the formation of polar orthorhombic phase (o-phase) HfO_2, which has been achieved by doping elements in combination with a post-rapid thermal annealing (RTA) treatment.[2,5–9] However, the crystallization of polar o-phase HfO_2 is less competitive, which greatly limits the ferroelectricity. Generally, the growth of improved ferroelectric HfO_2 thin films needs careful control of the oxygen vacancy (V_O) defects in HfO_2 thin films. As reported, HfO_2 prefers to crystallize into either nonpolar monoclinic phase (m-phase) or tetragonal phase (t-phase),[8] which can structurally transform to polar o-phase with the assistance of V_O.[10–12] However, the facile migration of V_O in turn deteriorates the ferroelectricity.[13–15] Although great efforts focusing on the modulation of V_O have been made in recent years,[16–19] additional strategies still need to be explored to further improve the ferroelectricity of the as-grown HfO_2 thin films.

It has been noticed that the ferroelectricity was substantially enhanced when capping a layer onto HfO_2 thin films, which promoted the structural transition to polar o-phase HfO_2 owing to interfacial stresses induced by lattice and thermal-expansion coefficient mismatches between HfO_2 and the capping layer.[9,20–22] Recently, the effects of strains on the formation of polar o-phase have been theoretically studied.[23–27] It is suggested that nonpolar t-phase can structurally transformed to polar $Pnm2_1$ phase when the HfO_2 suffers from in-plane-shear strains.[25] In addition, the structural transition from nonpolar m-phase to polar o-phase occurs when compressive stress is imposed on HfO_2.[24,26] Furthermore, the o-phase should be further thermally stabilized by appropriate stresses. However, efforts involving interfacial stress engineering have seldom been made in the synthesis of ferroelectric HfO_2 thin films so far.[28,29] The preliminary results suggested that the HfO_2 thin films grown on different substrates showed distinct crystallization behaviors. Typically, HfO_2 thin films were mainly crystallized into nonpolar m-phase on relaxed and compressively strained $La_{0.67}Sr_{0.33}MnO_3$ (LSMO) layers, whereas they were crystalized into polar o-phase on tensile strained LSMO layers.[28] Consequently, we herein explore the synthesis of ferroelectric Al doped HfO_2 (HfO_2:Al) thin films on various oriented Si substrates. It is shown that m-

†Corresponding author. E-mail: andychain@live.cn

© 2024 Chinese Physical Society and IOP Publishing Ltd

phase HfO_2 grown on (111)-oriented Si suffered from highly compressive strains, promoting the crystallization of o-phase HfO_2 and resulting in improved ferroelectricity with a remnant polarization ($2P_r$) as high as 26.7 μC/cm^2.

2. Experiments

The HfO_2:Al thin films with a 5.0 mol% Al doping and a thickness of 13.4 nm were grown on (100), (110), and (111)-oriented low resistivity (< 0.001 Ω·cm) p-type Si substrates using atomic layer deposition (ALD) method. Briefly, the Si substrates were cleaned with HF acid to remove the natural oxide layer, then by acetone, alcohol, and deionized water in sequence. To avoid batch-to-batch variations, the (100), (110), and (111)-oriented Si substrates were placed closely together in the ALD growth chamber. Tetrakis (dimethylamino) hafnium (IV), trimethyl aluminum, and water were used as Hf, Al, and O sources, respectively. The 5.0 mol% Al doping was realized by setting the cycle ratio of Hf and Al source pulses as 19:1. The growth temperature is 250 °C. Crystallization of HfO_2:Al thin films was realized by a post-RTA treatment at 950 °C for 60 s in N_2 with a quartz tube furnace. In detail, the 950 °C was first reached before the annealing, the samples were then transferred to the furnace via a magnetic conveyor. Finally, the samples were pulled out from the furnace after 60 s.

The surface roughness of Si substrates and HfO_2:Al thin films were investigated by atomic force microscope (AFM, MFP-3D). The structural properties of HfO_2:Al thin films were studied by grazing incidence x-ray diffraction (GIXRD, BrukerD8 Advance). The ferroelectricity of HfO_2:Al thin films was characterized by polarization–electric field (P–E) hysteresis loop measurements at a frequency of 1000 Hz (TF Analyzer 2000).

3. Results and discussion

We first show the surface roughness of HfO_2:Al thin films. Figures 1(d)–1(f) show the AFM images of RTA-treated HfO_2:Al thin films prepared on differently-oriented Si substrates. The results seem to suggest that the growth of HfO_2:Al thin films smooth the surface of Si substrates (Figs. 1(a)–1(c)). Notably, the HfO_2:Al thin films exhibit distinct surface roughness. As illustrated, the HfO_2:Al thin films grown on (100) and (111)-oriented Si substrates exhibit a smooth surface with a root-mean-square (RMS) roughness of 0.46 nm and 0.25 nm, respectively (Figs. 1(d)–1(e)). A smooth surface is critical for the growth of ferroelectric HfO_2 thin films at an ultra-thin thickness and the subsequent fabrication of Moore-beyond ferroelectric HfO_2 thin films-based devices. In contrast, the HfO_2:Al thin films synthesized on (110)-oriented Si substrate show a rough surface with a RMS roughness of 0.63 nm (Fig. 1(f)). As discussed below, the reduced surface roughness of HfO_2:Al thin films grown on (111)-oriented Si substrate is attributed to the low lattice mismatch between (111)-oriented o-phase HfO_2 and (111)-oriented Si substrate.

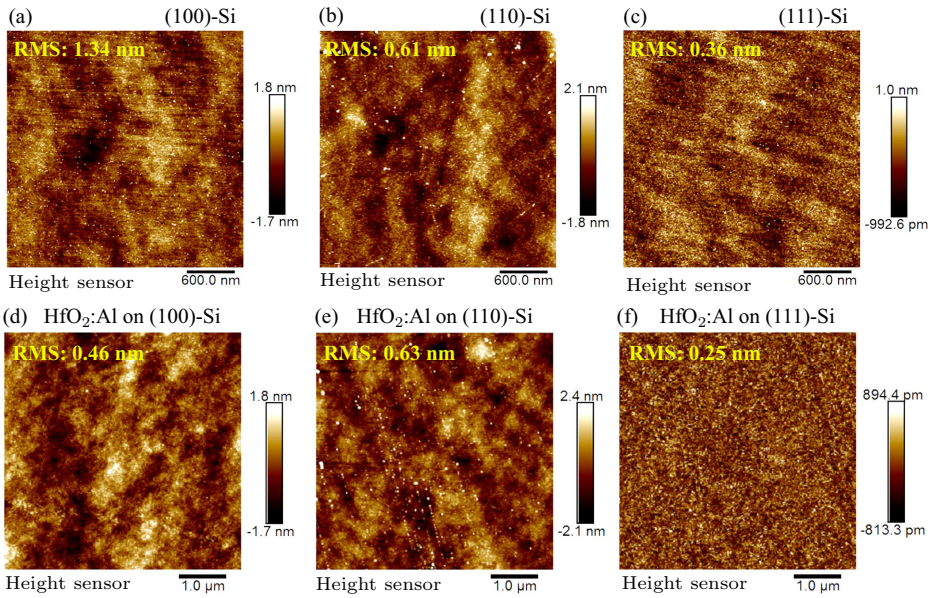


Fig. 1. Surface roughness of Si substrates and HfO_2:Al thin films. AFM images of (a)–(c) Si substrates and (d)–(f) HfO_2:Al thin films.

Figure 2(a) illustrates the GIXRD patterns of HfO_2:Al thin films prepared on (100), (110), and (111)-oriented Si substrates. As shown, the GIXRD peaks are observed at around 24.97°, 28.91°, 30.96°, 35.73°, and 41.55°, which could be ascribed to $(110)_m$, $(-111)_m$, $(111)_o$, $(200)_m$, and $(-211)_m$ planes, respectively, where the subscripts denote the lattice structure of HfO_2. The emergence of $(111)_o$ peak may suggest the formation of (111)-oriented polar o-phase HfO_2 within

the HfO_2:Al thin films, which is mainly attributed to the Al doping.[12] Notably, theoretical studies suggested that polar o-phase HfO_2 at its optimal equilibrium strains is thermodynamically more stable than the m-phase HfO_2 in (111)-oriented thin films.[24] In addition, o-phase HfO_2 adopts the (111)-orientation may display a large remnant polarization.[6,30] However, the 30.96° peak may also be assigned as $(011)_t$, which implies the formation of nonpolar t-phase HfO_2. In fact, it is difficult to distinguish the o-phase and t-phase from GIXRD patterns, since the GIXRD peaks are too broad to resolve the $(011)_t$ (30.06°) and $(111)_o$ (29.86°) accurately.[31] Importantly, theoretical calculations have suggested that nonpolar m-phase facilely transformed to polar o-phase when HfO_2 thin films suffered from compressive strains (as verified from GIXRD, shown below).[24] As a result, the chances of crystallization of nonpolar t-phase should be low, especially in the HfO_2:Al thin films grown on (100) and (111)-oriented Si substrates.

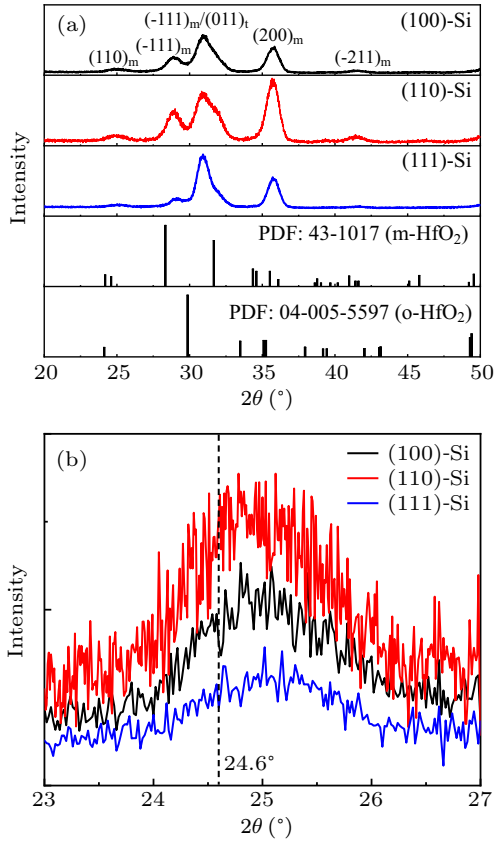


Fig. 2. GIXRD patterns of HfO_2:Al thin films. Data shown in (b) were extracted from (a). The dashed black line in (b) shows the position of XRD peak of $(110)_m$ according to PDF card: 43-1017.

Further studies show that the GIXRD patterns of these HfO_2:Al thin films shift to a high angel side compared to the standard PDF card, which is due to Al doping and HfO_2/Si interfacial stress induced by the lattice and thermal-expansion coefficient mismatches between HfO_2 and Si substrates (Table 1). Typically, Fig. 2(b) shows the $(110)_m$ GIXRD peak of HfO_2:Al thin films synthesized on (100), (110), and (111)-oriented Si substrates, showing that m-phase HfO_2:Al thin films suffer from compressive strains. According to Refs. [24,26] where the compressive stress promoted the nonpolar m-phase to polar o-phase transition, it seems that m-phase HfO_2:Al films grown on (100), (110), and (111)-oriented Si substrates have a chance to crystallize into polar o-phase. However, the m-phase HfO_2:Al thin films synthesized on (100), (110), and (111)-oriented Si substrates show distinct degrees of compressive strain. As shown, the m-phase HfO_2:Al thin films suffer from a strong compressive strain on (111)-oriented Si substrate, but a weak one on (110)-oriented Si substrate. As a result, a promoted crystallization of polar o-phase HfO_2 and an enhanced ferroelectricity in the HfO_2:Al thin films synthesized on (111)-oriented Si substrate can be expected.

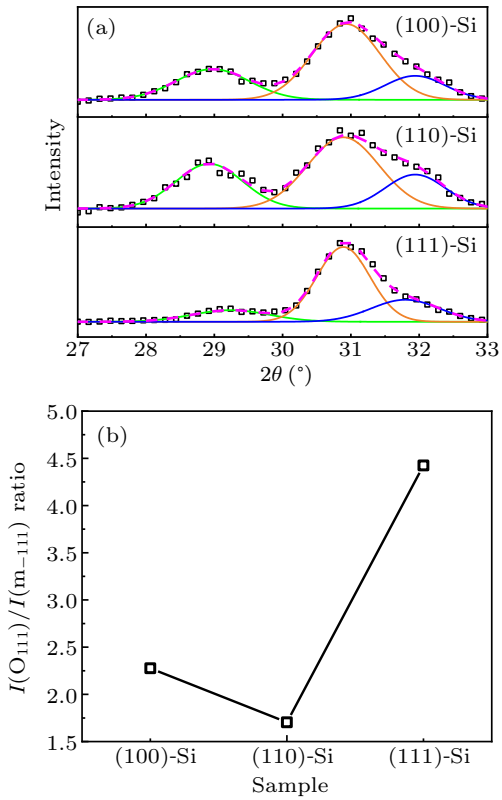


Fig. 3. Crystallization behaviors of HfO_2:Al thin films. (a) Fitting of GIXRD patterns. The square hollows and colorful lines are raw and fitting data, respectively. The data were extracted from Fig. 2(a). (b) Relative intensity of $(111)_o$ peak of HfO_2:Al thin films.

However, remarkable nonpolar m-phase HfO_2 is observed within the HfO_2:Al thin films (Fig. 2(a)), which should lower the ferroelectricity. This might be attributed to the limitations of ALD method in the elements doping process, where the mother materials (Hf and O) and dopant (Al) were alternately pumped into the growth chamber. Notably, the GIXRD patterns have further suggested that HfO_2:Al thin films grown on differently-oriented Si substrates exhibit distinct crystallization behaviors. In brief, the content of polar o-phase HfO_2 in the HfO_2:Al thin films on differently-oriented Si substrates varies (Fig. 3). Herein, the content of polar o-phase HfO_2 was

analyzed from relative intensity of $(111)_o$ GIXRD peak, i.e., $I(o_{111})/I(m_{-111})$ ratio, where the $I(o_{111})$ and $I(m_{-111})$ are the integrated intensities of $(111)_o$ and $(-111)_m$ GIXRD peaks, respectively. To obtain the $I(o_{111})$ and $I(m_{-111})$ values accurately, the GIXRD peaks were fitted by Gaussian multi-peaks-fitting method,[32] and the results are depicted in Fig. 3(a). The relative intensities of $(111)_o$ GIXRD peak of HfO_2:Al thin films grown on differently-oriented Si substrates are illustrated in Fig. 3(b). The HfO_2:Al thin films grown on (111)-oriented Si substrate show the strongest relative intensity of $(111)_o$ GIXRD peak, implying the highest content of o-phase in the HfO_2:Al thin films. This suggests that the crystallization of polar o-phase HfO_2 is promoted when HfO_2 were grown on (111)-oriented Si substrate. However, the relative intensity of $(111)_o$ GIXRD peak is decreased in HfO_2:Al thin films grown on (110)-oriented Si substrate, suggesting the suppressed crystallization of polar o-phase HfO_2. It is supposed that the HfO_2:Al thin films grown on (110)-oriented Si substrate mainly crystallized into t-phase according to the *P*–*E* results shown below, which may be understood as follows: the HfO_2:Al thin films on (110)-oriented Si substrates suffer from a weak compressive strain (as shown in Fig. 2(b)), which may be unable to support the structural transition from m-phase to o-phase. Instead, structural transition from m-phase to t-phase has occurred, which is attributed to the increased surface energy of m-phase[33–36] and improved thermal stabilities of t-phase in ultra-thin films.[33,37] It is worth noting that the promoted crystallization of polar o-phase concluded from Fig. 3 are well consistent with the shifts of GIXRD peaks shown in Fig. 2(b), provided that the structural transition from m-phase to o-phase is attributed to both the compressive strain imposed on m-phase HfO_2 thin films and the generation of V_O.[24,38]

Figures 4(a) and 4(b) illustrate the *P*–*E* and corresponding current–electric field (*I*–*E*) curves of HfO_2:Al thin films grown on differently-oriented Si substrates. As depicted, the HfO_2:Al thin films grown on differently-oriented Si substrates exhibit distinct ferroelectricity. In detail, typical ferroelectric hysteresis loop (Fig. 4(a)) and remarkable current peaks (Fig. 4(b)) induced by the polarization switching have been observed in the HfO_2:Al thin films grown on (100) and (111)-oriented Si substrates, showing that these HfO_2:Al thin films are ferroelectric. Furthermore, the preliminary results show that the HfO_2:Al thin films grown on (111)-oriented Si substrate show improved ferroelectricity with a remanent polarization ($2P_r$) of 29.7 μC/cm^2, which is higher than those grown on (100)-oriented Si substrate (19.4 μC/cm^2) (Fig. 4(a)).

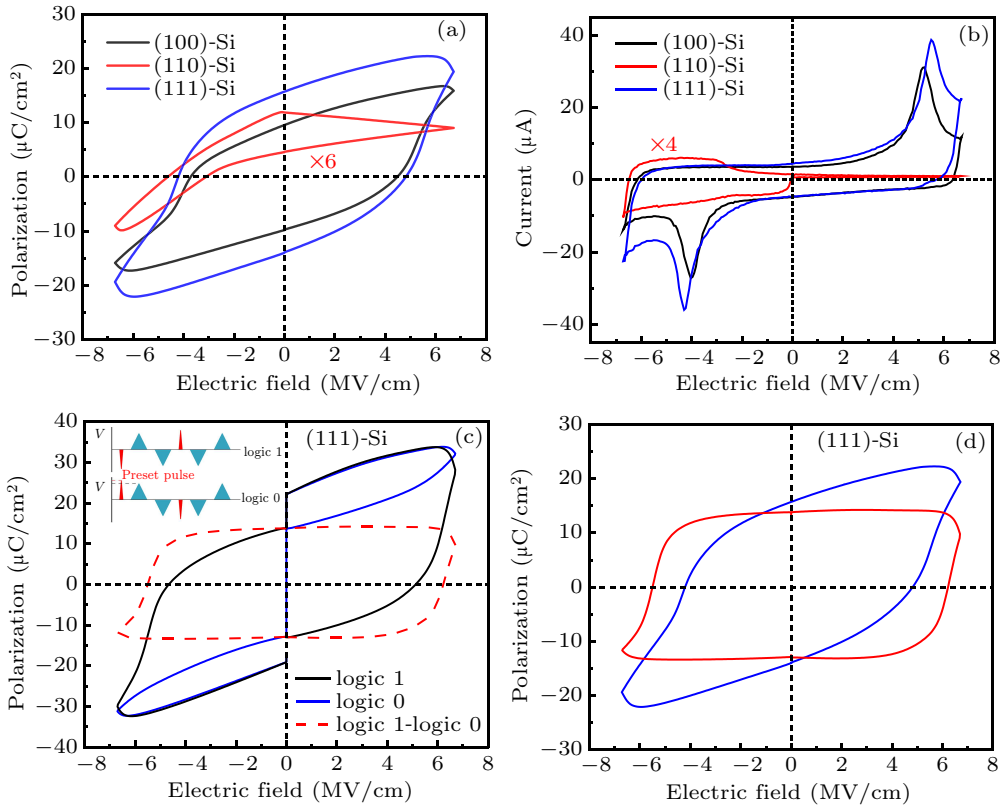


Fig. 4. Ferroelectricity of HfO_2:Al thin films. (a) *P*–*E*. (b) *I*–*E*. (c) True-remanent and non-remanent hysteresis loops. (d) Traditional (blue line) and remanent-only (red line) hysteresis loops. The thicknesses of HfO_2:Al thin films are 13.4 nm.

However, leakage current was observed in the *I*–*E* curves (Fig. 4(b)), which is caused by the diffusion of V_O under an applied electric field.[15] This led to unwanted spurious data in the *P*–*E* measurements. Generally, the total polarization in a *P*–*E* hysteresis curve consists of contributions from both the "true-remanent" and "non-remanent (typically, the leak-

age component)" components. To eliminate the non-remanent components, two different series of triangular pulse voltages were introduced, as depicted in Fig. 4(c). In detail, logic 1 loop includes switched (true-remanent) and unswitched (non-remanent) polarization (black line), while logic 0 loop only contains unswitched polarization (blue line). Finally, subtracting logic 0 from logic 1 obtains the true-remnant polarization (red dashed line). Figure 4(d) illustrates the traditional (blue line) and remanent-only (red line) hysteresis loops of HfO_2:Al thin films grown on (111)-oriented Si substrates. As shown, a small difference in the remnant polarization value has been observed, which tends to increase with an increase in the external electric field.

Figures 5(a) and 5(b) exhibit the corrected *P*–*E* and *I*–*E* curves of HfO_2:Al thin films grown on differently-oriented Si substrates. As shown, the remnant polarization is 26.7 μC/cm^2 and 17.4 μC/cm^2 for HfO_2:Al thin films prepared on (111) and (110)-oriented Si substrates, respectively. This shows that the ferroelectricity of HfO_2:Al thin films can be improved by interfacial stress engineering via employing a selective substrate. This obviously is a simple pathway compared to modulation of V_O, where the latter widely involved careful control of the thermodynamical conditions during the growth[12,18,39] and post-treatments.[16,40] In contrast, the HfO_2:Al thin films grown on (110)-oriented Si substrate are non-ferroelectric. Figure 5(c) depicts the statistical data of accurate remnant polarization of HfO_2:Al thin films synthesized on (100) and (111)-oriented Si substrates, where the enhanced ferroelectricity in the HfO_2:Al thin films grown on (111)-oriented Si substrate is confirmed. It is speculated that the enhanced ferroelectricity is mainly caused by the promoted crystallization of o-phase HfO_2 benefiting from the interfacial compressive stress, which has been verified from previous reports on ferroelectric $Hf_{0.5}Zr_{0.5}O_2$ thin films grown on tensile strained[28] and MnO_2-terminated[41] LSMO layers.

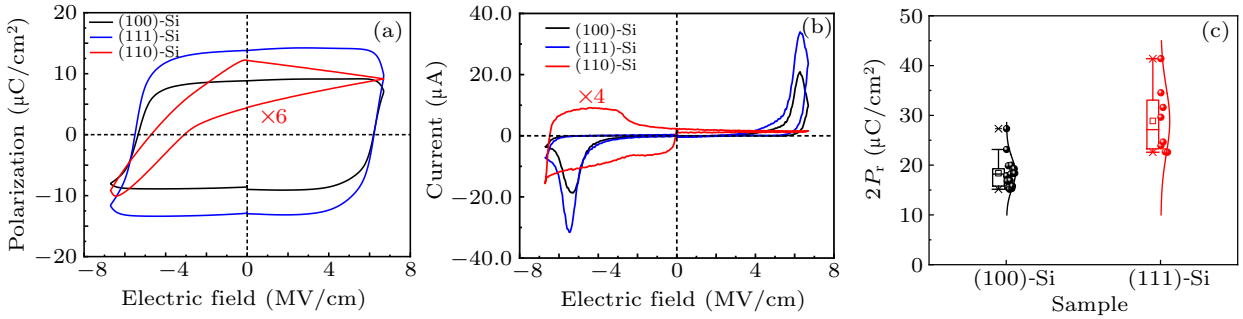


Fig. 5. Characterizations of ferroelectricity of HfO_2:Al thin films. (a) Remanent-only *P*–*E*. (b) Remanent-only *I*–*E*. (c) Statistics of the remnant polarization.

Table 1. Lattice constants and thermal-expansion coefficient of m/o-phase HfO_2 and Si.

Materials	Lattice constants	Thermal-expansion coefficient at 950 °C (10^{-6} K^{-1})
m-phase HfO_2	$a = 5.14$ Å, $b = 5.19$ Å, $c = 5.32$ Å $\alpha = 90°$, $\beta = 99.8°$, $\gamma = 90°$	$\alpha_a = 9.34$, $\alpha_b = 2.98$, $\alpha_c = 13.1$[42]
o-phase HfO_2	$a = 5.04$ Å, $b = 5.07$ Å, $c = 5.26$ Å, $\alpha = \beta = \gamma = 90°$	/
Si	$a = b = c = 5.47$ Å, $\alpha = \beta = \gamma = 90°$	~ 4.33[43]

Finally, the mechanisms of the formation of polar o-phase HfO_2 within the HfO_2:Al thin films are briefly discussed. It has been shown that the crystallization of HfO_2 occurred during the RTA process,[12] where the nucleation of HfO_2 was preferred at the Si surface owing to the wettability of Si surface. Because of the lattice and coefficient of thermal-expansion mismatches between the m-phase HfO_2 and Si substrate (Table 1), m-phase HfO_2 suffers from out-plane compressive strains. As a result, structural transition from m-phase to o-phase occurs due to the lower free energy of compressively strained (111)-oriented o-phase than that of m-phase.[24] In addition, doping of Al facilitates the formation of V_O,[12] which further promotes the structural transition.[12,16] Meanwhile, the stabilities of o-phase may depend on lattice mismatch between the (111)-oriented o-phase HfO_2 and Si substrates, according to previous reports on the preparation of cubic ZnO[44] and hexagonal ε-Ga_2O_3.[45] Interestingly, the in-plane lattice of (111)-oriented o-phase HfO_2 matches well with that of (111)-oriented Si substrate (Figs. 6(a) and 6(d)), showing that the polar o-phase can be thermally stabilized by the underneath (111)-oriented Si substrate, which further promoted the crystallization of o-phase HfO_2. In comparison, the lattice mismatch between (111)-oriented o-phase HfO_2 and (100)-oriented Si substrate is high, but fortunately it can be reduced when the o-phase HfO_2 in-plane rotates by 45° (Fig. 6(b)). As a result, o-phase HfO_2 formed within the HfO_2:Al thin films synthesized on (100)-oriented Si substrate. However, the lattice mismatch between (111)-oriented o-phase

HfO_2 and (110)-oriented Si substrates is high (Fig. 6(c)), which suppressed the crystallization of o-phase HfO_2. Instead, structural transition from m-phase to t-phase has more chance.

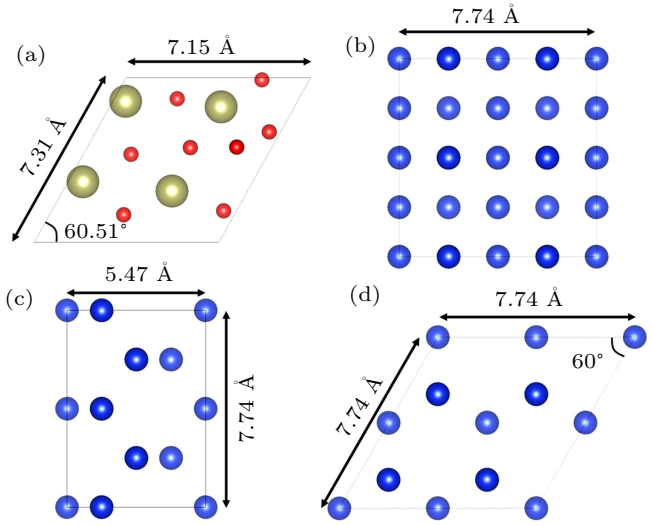


Fig. 6. In-plane atomic alignments of o-phase HfO_2 and Si. (a) (111)-oriented o-phase HfO_2, (b) (100)-oriented Si, (c) (110)-oriented Si, and (d) (111)-oriented Si. The yellow, red, and blue spheres are Hf, O and Si atoms, respectively.

4. Conclusion and perspectives

Enhanced ferroelectricity of HfO_2:Al thin films have been prepared on (111)-oriented Si substrate. Owing to the lattice and coefficient of thermal-expansion mismatches between m-phase HfO_2 and Si substrates, the m-phase HfO_2:Al thin films suffered from compressive strains, which promoted the structural transition from nonpolar m-phase to polar o-phase HfO_2. Furthermore, the in-plane lattice of (111)-oriented o-phase HfO_2 matches with that of (111)-oriented Si, which further thermally stabilized the polar o-phase HfO_2. As a result, the crystallization of o-phase HfO_2 was promoted within the HfO_2:Al thin films grown on (111)-oriented Si substrate, which resulted in an enhanced ferroelectricity with a remnant polarization as high as 26.7 $\mu C/cm^2$. The results provide a simple pathway for the synthesis of improved ferroelectric HfO_2 thin films in the future.

Data availability statement

The data that support the findings of this study are available from the corresponding author upon reasonable request.

Acknowledgements

Research Fund of Guangdong–Hong Kong–Macao Joint Laboratory for Intelligent Micro-Nano Optoelectronic Technology, China (Grant No. 2020B1212030010) and Project of Faculty of Agricultural Equipment of Jiangsu University (Grant No. NZXB20210202) are acknowledged.

References

[1] Schroeder U, Park M H, Mikolajick T and Hwang C S 2022 *Nat. Rev. Mater.* **7** 653
[2] Müller J, Böscke T S, Bräuhaus D, Schröder U, Böttger U, Sundqvist J, Kücher P, Mikolajick T and Frey L 2011 *Appl. Phys. Lett.* **99** 112901
[3] Yurchuk E, Muller J, Hoffmann R, Paul J, Martin D, Boschke R, Schlosser T, Muller S, Slesazeck S, Bentum R, Trentzsch M, Schröder U and Mikolajick T 2012 *4th IEEE International Memory Workshop*, 20–23 May 2012 p. 1
[4] Si M, Saha A K, Gao S, Qiu G, Qin J, Duan Y, Jian J, Niu C, Wang H, Wu W, Gupta S K and Ye P D 2019 *Nat. Electron.* **2** 580
[5] Mueller S, Mueller J, Singh A, Riedel S, Sundqvist J, Schroeder U and Mikolajick T 2012 *Adv. Funct. Mater.* **22** 2412
[6] Yun Y, Buragohain P, Li M, Ahmadi Z, Zhang Y, Li X, Wang H, Li J, Lu P, Tao L, Wang H, Shield J E, Tsymbal E Y, Gruverman A and Xu X 2022 *Nat. Mater.* **21** 903
[7] Kozodaev M G, Chernikova A G, Korostylev E V, Park M H, Schroeder U, Hwang C S and Markeev A M 2017 *Appl. Phys. Lett.* **111** 132903
[8] Böscke T S, Müller J, Bräuhaus D, Schröder U and Böttger U 2011 *Appl. Phys. Lett.* **99** 102903
[9] Lomenzo P D, Zhao P, Takmeel Q, Moghaddam S, Nishida T, Nelson M, Fancher C M, Grimley E D, Sang X, LeBeau J M and Jones J L 2014 *J. Vac. Sci. Technol. B* **32** 03D123
[10] Zhou Y, Zhang Y K, Yang Q, Jiang J, Fan P, Liao M and Zhou Y C 2019 *Comp. Mater. Sci.* **167** 143
[11] Rushchanskii K Z, Blügel S and Ležaić M 2021 *Phys. Rev. Lett.* **127** 087602
[12] Chen S, Qin P, Yang J, Chen M, Du Q, Kong Y, Liu Y and Cao D 2023 *J. Alloys Compd.* **965** 171456
[13] Lee J C, Oh S J, Cho M, Hwang C S and Jung R 2004 *Appl. Phys. Lett.* **84** 1305
[14] Chen H, Tang L, Liu L B X, Chen Y, Luo H, Yuan X and Zhang D 2021 *Appl. Surf. Sci.* **542** 148737
[15] Starschich S, Menzel S and Böttger U 2016 *Appl. Phys. Lett.* **108** 032903
[16] Kang S, Jang W, Morozovska A N, Kwon O, Jin Y, Kim Y H, Bae H, Wang C, Yang S H, Belianinov A, Randolph S, Eliseev E A, Collins L, Park Y, Jo S, Jung M H, Go K J, Cho H W, Choi S Y, Jang J H, Kim S, Jeong H Y, Lee J, Ovchinnikova O S, Heo J, Kalinin S V, Kim Y M and Kim Y 2022 *Science* **376** 731
[17] Su M, Liu J, Weng Z, Ding X, Chen Z, Zhang Y, Zhao L, Lee C and Zhao Y 2021 *Appl. Phys. Express* **14** 126503
[18] Pal A, Narasimhan V K, Weeks S, Littau K, Pramanik D and Chiang T 2017 *Appl. Phys. Lett.* **110** 022903
[19] Su M, Gao S, Weng Z, Zhao L, Lee C and Zhao Y 2022 *IEEE Electr. Device Lett.* **43** 1057
[20] Szyjka T, Baumgarten L, Mittmann T, Matveyev Y, Schlueter C, Mikolajick T, Schroeder U and Müller M 2020 *ACS Appl. Electron. Mater.* **2** 3152
[21] Cao R, Wang Y, Zhao S, Yang Y, Zhao X, Wang W, Zhang X, Lv H, Liu Q and Liu M 2018 *IEEE Electr. Device Lett.* **39** 1207
[22] Huo S, Zheng J, Liu Y, Li Y, Tao R, Lu X and Liu J 2023 *Chin. Phys. B* **32** 127701
[23] Batra R, Huan T D, Jones J L, Rossetti G J and Ramprasad R 2017 *J. Phys. Chem. C* **121** 4139
[24] Liu S and Hanrahan B M 2019 *Phys. Rev. Mater.* **3** 054404
[25] Qi Y, Singh S, Lau C, Huang F T, Xu X, Walker F J, Ahn C H, Cheong S and Rabe K M 2020 *Phys. Rev. Lett.* **125** 257603
[26] Fan S T, Chen Y W and Liu C W 2020 *J. Phys. D Appl. Phys.* **53** 23LT01
[27] Behara S S and Van der Ven A 2022 *Phys. Rev. Mater.* **6** 054403
[28] Estandía S, Dix N, Gazquez J, Fina I, Lyu J, Chisholm M F, Fontcuberta J and Sánchez F 2019 *ACS Appl. Electron. Mater.* **1** 1449
[29] Song T, Tan H, Estandía S, Gàzquez J, Gich M, Dix N, Fina I and Sánchez F 2022 *Nanoscale* **14** 2337
[30] Wei Y, Nukala P, Salverda M, Matzen S, Zhao H J, Momand J, Everhardt A S, Agnus G, Blake G R, Lecoeur P, Kooi B J, Íñiguez J, Dkhil B and Noheda B 2018 *Nat. Mater.* **17** 1095

[31] Zhang Y, Wang D, Luo C, Cheng J, Huo S, Zhang B, Tao R, Chen D, Fan Z, Dai J Y, Lu X and Liu J M 2022 *IEEE T. Electron Dev.* **69** 3094
[32] Xiao D Q, Luo B B, Xiong W, Wu X, Zhang D W and Ding S J 2021 *IEEE T. Electron Dev.* **68** 6359
[33] Batra R, Tran H D and Ramprasad R 2016 *Appl. Phys. Lett.* **108** 172902
[34] Materlik R, Künneth C and Kersch A 2015 *J. Appl. Phys.* **117** 134109
[35] Park M H, Lee Y H, Kim H J, Schenk T, Lee W, Kim K D, Fengler F P G, Mikolajick T, Schroeder U and Hwang C S 2017 *Nanoscale* **9** 9973
[36] Mimura T, Shimizu T, Sakata O and Funakubo H 2021 *Phys. Rev. Mater.* **5** 114407
[37] Shimizu T, Katayama K, Kiguchi T, Akama A, Konno T J and Funakubo H 2015 *Appl. Phys. Lett.* **107** 032910
[38] Deng Y, Yang W, Lin X, Liao N, Zhu B, Yang Q, Jiang J and Jiang L 2023 *Comp. Mater. Sci.* **221** 112036
[39] Kashir A, Oh S and Hwang H 2021 *Adv. Eng. Mater.* **23** 2000791
[40] Lee K, Park K, Lee H, Song M S, Lee K C, Namkung J, Lee J H, Park J and Chae S C 2021 *Sci. Rep.* **11** 6290
[41] Shi S, Xi H, Cao T, Lin W, Liu Z, Niu J, Lan D, Zhou C, Cao J, Su H, Zhao T, Yang P, Zhu Y, Yan X, Tsymbal E Y, Tian H and Chen J 2023 *Nat. Commun.* **14** 1780
[42] Patil R N and Subbarao E C 1969 *J. Appl. Crystallogr.* **2** 281
[43] Okada Y and Tokumaru Y 1984 *J. Appl. Phys.* **56** 314
[44] Kim S K, Jeong S Y and Cho C R 2003 *Appl. Phys. Lett.* **82** 562
[45] Cho S B and Mishra R 2018 *Appl. Phys. Lett.* **112** 162101